



Microstructure, Dielectric and Piezoelectric Properties of Nd-Doped $\text{Bi}_4\text{Ti}_3\text{O}_{12}$ Ceramics

Sergei V. Zubkov^{1,1}(✉), Ivan A. Parinov², Alexander V. Nazarenko³,
and Yulia A. Kuprina¹

¹ Research Institute of Physics, Southern Federal University, Rostov-On-Don, Russia
svzubkov61@mail.ru

² I. I. Vorovich Mathematics, Mechanics and Computer Sciences Institute, Southern Federal
University, Rostov-On-Don, Russia

³ Federal Research Centre, The Southern Scientific Centre of the Russian Academy of Sciences,
Rostov-On-Don, Russia

Abstract. In this paper, a series of Aurivillius phase (AP) $\text{Bi}_{4-x}\text{Nd}_x\text{Ti}_3\text{O}_{12}$ ($x = 0.0, 0.2$) ceramics, prepared in a solid reaction process and sintered at different temperatures (1000 ~ 1050 °C), are investigated. Their dielectric and piezo properties are studied. The piezoelectric modulus, crystal lattice parameters and Curie temperature were measured for all of studied compounds. The results of the study of the microstructure show that the average size of BNT ceramic grains remains with increasing sintering temperature. It was found that the relative permittivity increased by almost 1.5 times with the increasing of sintering temperature to 1050 °C.

Keywords: Aurivillius phase (AP) · Microstructure · $\text{Bi}_{4-x}\text{Nd}_x\text{Ti}_3\text{O}_{12}$ ·
Activation energy (E_a) · Curie temperature (T_C) · Piezoelectric modulus (d_{33})

1 Introduction

In 1949, while studying the $\text{Bi}_2\text{O}_3 - \text{TiO}_2$ system, V. Aurivillius established the formation of $\text{Bi}_4\text{Ti}_3\text{O}_{12}$ (BTO) oxide with a perovskite type structure [1]. Only ten years later, after the discovery by G. Smolensky, V. Isupov and A. Agranovskaya of the ferroelectric properties of $\text{Bi}_2\text{PbNbO}_9$, which belongs to this class of compounds [2], a new stage of study began. Aurivillius phases (APs) form a large family of bismuth-containing layered compounds of the perovskite type, the chemical composition of which is described by the general formula: $A_{m-1}\text{Bi}_2\text{B}_m\text{O}_{3m+3}$. The crystal structure of AP consists of alternating $[\text{Bi}_2\text{O}_2]^{2+}$ layers, separated by m perovskite-like layers $[\text{A}_{m-1}\text{B}_m\text{O}_{3m+1}]^{2-}$, where A are the ions with large radii have dodecahedral coordination, and B -positions inside oxygen octahedra are occupied by highly charged ($\geq 3+$) cations with a small radius. The value of m is determined by the number of perovskite layers $[\text{A}_{m-1}\text{B}_m\text{O}_{3m+1}]^{2-}$, located between the fluorite-like $[\text{Bi}_2\text{O}_2]^{2+}$ layers, and can take an integer or half-integer values in the range of 1 – 6 (see Fig. 1, $m = 3$).

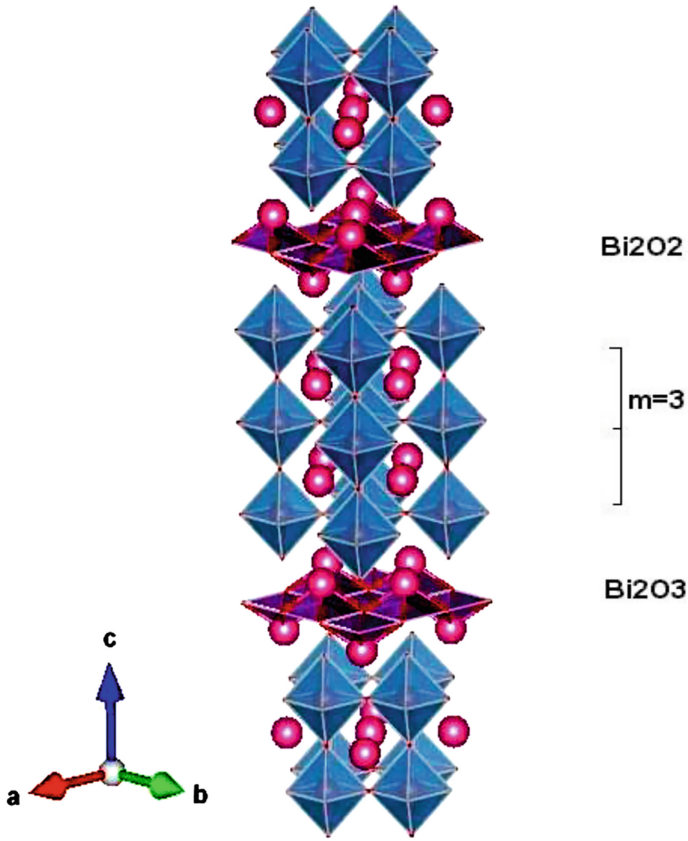


Fig. 1 Aurivillius phase structure: $m = 3$

The layered ferroelectrics of the Aurivillius phase family (APF) attract much attention due to their high Curie temperature (T_C) [3, 4]. The structure of APF $\text{Bi}_2A_{m-1}B_m\text{O}_{3m+3}$ compounds is tetragonal above the Curie point T_C and belongs to the space group $I4/mmm$. The type of space group below the Curie point T_C depends on the value of m : $B2cb$ or $Pca2_1$ for odd m ; $A2_1am$ for even m ; $Cmm2$ or $I2cm$ for half-integer m .

In the AP, much attention was paid to the BTO compound. It is believed to have potential applications in high-temperature piezoelectric devices and ferroelectric memory devices. It has large spontaneous polarization (P_s) $\sim 50 \mu\text{C}/\text{cm}^2$ [5–7], high piezoelectric modulus [8] and high Curie temperature (T_C) $\sim 675^\circ\text{C}$ [9]. In this work, bismuth ions Bi^{3+} in the A-position were doped with neodymium ions Nd^{3+} . It was indicated in early studies of $\text{Bi}_3\text{Ti}_{1.5}\text{W}_{0.5}\text{O}_9$ ceramics that doping of A-position with the Nd^{3+} rare earth ion improves the piezoelectric activity and reduces the number of oxygen vacancies [10].

Ceramics of $\text{Bi}_{4-x}\text{Nd}_x\text{Ti}_3\text{O}_{12}$ ($x = 0.0, 0.2$) was synthesized by the solid-phase reaction method. The crystal structure, microstructure, dielectric properties, piezoelectric properties of ceramics have been studied.

2 Experiment

Polycrystalline samples $\text{Bi}_{4-x}\text{Nd}_x\text{Ti}_3\text{O}_{12}$ ($x = 0.0, 0.2$) with APF structure were synthesized by the solid-state reaction of the Bi_2O_3 , Nd_2O_3 , TiO_2 corresponding oxides. All initial compounds were analytical grade. After weighing in accordance with the stoichiometric composition and thorough grinding of the initial oxides with the addition of ethanol, the pressed samples were calcined at a temperature of 750°C for 4 h. The samples were fired in a laboratory muffle furnace in air. Then the sample was crushed, repeatedly crushed and pressed into tablets of 10 mm in diameter and 1.0 – 1.5 mm thickness, followed by final synthesis at a temperature of $1000 \sim 1050^\circ\text{C}$ (for 2 h).

The X-ray pattern was recorded on a Rigaku Ultima IV diffractometer with a Cu X-ray tube. The $\text{Cu}_{K\alpha 1, \alpha 2}$ radiation was separated from the total spectrum using a Ni-filter. The X-ray pattern was measured in the range of 2θ angles from 10° to 80° with a scan step of 0.02° and an exposure (intensity registration time) of 4 s per point. Analysis of the X-ray pattern profile, determining the position of the lines, their indexing (hkl), and refinement of the unit cell parameters were carried out using the PCW 2.3 program [11].

To measure the permittivity and electrical conductivity, electrodes were deposited on flat surfaces of APF samples in the form of disks of 10 mm in diameter and about 1.5 mm thick using Ag paste, annealed at a temperature of 650°C (20 min.). The temperature and frequency dependences of the dielectric characteristics were measured using an E7–20 immittance meter in the frequency range from 100 kHz to 1 MHz and in the temperature range from room temperature to 750°C . The sample was subjected to polarization in an oil bath at 145°C at a voltage of 35 kV/cm for 30 min. Microstructure images of $\text{Bi}_{4-x}\text{Nd}_x\text{Ti}_3\text{O}_{12}$ ($x = 0.0, 0.2$) were obtained using a Carl Zeiss EVO 40 scanning electron microscope (SEM) (Germany) at the Center for Collective Use of the SSC RAS (No 501994). The study was carried out on mechanical cleavages of the fabricated ceramics. In the absence of an additional conductive layer, grain smearing and multiple charge accumulation effects were observed. Therefore, to analyze the cleavage surface, the conductive layer was deposited using an SC7620 “MiniSputterCoater” magnetron sputtering setup. Before sputtering, the samples were not preliminarily subjected to mechanical treatment. The study was carried out in the regime of high accelerating voltage (EHT = 20 kV). To increase the resolution, the probe current was $I_{probe} = 55$ pA, and the work distance was $\text{WD} = 7 - 9$ mm.

3 Results and Discussion

Powder X-ray diffraction patterns of all studied $\text{Bi}_{4-x}\text{Nd}_x\text{Ti}_3\text{O}_{12}$ ($x = 0.0, 0.2$) solid solutions correspond to single-phase APF with $m = 3$ and do not contain additional reflections; they are isostructural to the known perovskite-like APF $\text{Bi}_{4-x}\text{Nd}_x\text{Ti}_3\text{O}_{12}$ ($x = 0.0, 0.2$) oxide. It was found that all synthesized APs crystallize in an orthorhombic system with unit cell space group B2cb. The X-ray diffraction patterns of all compounds

correspond to APF with $m = 3$. Figure 2 shows the experimental powder X-ray diffraction patterns of the compounds under study. All the diffraction peaks were indexed to the three-layered Aurivillius-type structure (JCPDS No. 72–1019).

The strongest diffraction peak was found as (117), and this agreed with the fact that the most intensive reflection of layered perovskites belonged to the type of $(112m + 1)$ [12]. Based on X-ray diffraction data, the parameters and volume of the unit cell were determined, they are shown in Table 1.

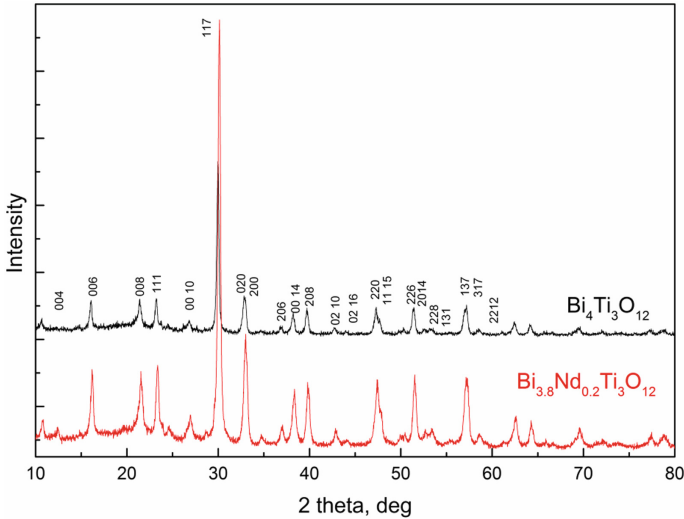


Fig. 2 XRD patterns of $\text{Bi}_{4-x}\text{Nd}_x\text{Ti}_3\text{O}_{12}$ ($x = 0.0, 0.2$) ceramics in the 2θ range of 10 – 80 °C

Table 1 Unit cell parameters a , b , c and volume V , tolerance-factor t , relative permittivity $\varepsilon'/\varepsilon_0$ at a frequency of 100 kHz, Curie temperature T_C , and activation energy E_a in various temperature regions

	Compound	a , Å	b , Å	c , Å	V , Å ³	t -factor	T_{C1050}/T_{C950}	$\varepsilon'_{1050}/\varepsilon'_{950}$
1	$\text{Bi}_4\text{Ti}_3\text{O}_{12}$	5.550	5.480	31.576	960.352	0.98	715/711	3800/2225
2	$\text{Bi}_{3.8}\text{Nd}_{0.2}\text{Ti}_3\text{O}_{12}$	5.436	5.418	31.756	935.286	0.978	685/680	2875/2195

The obtained unit cell parameters of the studied $\text{Bi}_{4-x}\text{Nd}_x\text{Ti}_3\text{O}_{12}$ ($x = 0.0, 0.2$) samples are close to those determined earlier for APF $\text{Bi}_4\text{Ti}_3\text{O}_{12}$: $a = 5.411$ Å, $b = 5.448$ Å, $c = 32.83$ Å. [13]. To obtain the degree of distortion of the ideal perovskite structure, we determined the tolerance factor t , which is presented in Table 1. The tolerance factor t was introduced by Goldschmidt [14] as a geometric criterion that determines the degree of stability and distortion of the crystal structure:

$$T = (R_A + R_O) / [(R_B + R_O)], \quad (1)$$

where R_A and R_B are the cation radii in positions A and B , respectively; R_O is the ionic radius of oxygen. In this work, the tolerance factor was calculated taking into account the Shannon ionic radii [15] for the corresponding coordination numbers (CN) (O^{2-} (CN = 6) $R_O = 1.40 \text{ \AA}$, Nd^{3+} (CN = 12) $R_{Nd^{3+}} = 1.27 \text{ \AA}$, Ti^{4+} (CN = 6) $R_{Ti^{4+}} = 0.605 \text{ \AA}$). Shannon did not give the Bi^{3+} ionic radius for coordination with CN = 12. Therefore, its value was determined from the ionic radius with CN = 8 ($R_{Bi^{3+}} = 1.17 \text{ \AA}$) multiplied by an approximation factor of 1.179, then for Bi^{3+} (CN = 12), we obtained $R_{Bi^{3+}} = 1.38 \text{ \AA}$. Table 2 shows the parameters of orthorhombic δb_0 and tetragonal $\delta c'$ deformation; average tetragonal period a_t and average thickness of one perovskite layer c' ; $c' = 3c/(8 + 6m)$ is the thickness of a single perovskite-like layer, $a_t = (a_0 + b_0)/(\sqrt{2})$ is the average value of the tetragonal period; a_0, b_0, c_0 are the lattice periods; $\delta c' = (c' - a_t)/a_t$ is the cell deviation from the cubic form, that is, elongation or contraction from the cubic form; $\delta b_0 = (b_0 - a_0)/a_0$ is the orthorhombic deformation, $c_0 = c/(2 + 1.5m)$, where $c/(2 + 1.5m)$ is the bismuth-oxygen layer thickness [16].

Table 2 V is the unit cell volume, a_t is the parameter of the tetragonal period, c' is the octahedron height along c -axis, $\delta c'$ is the deviation of the unit cell from the cubic shape, δb_0 is the rhombic distortion and c_0 is the bismuth – oxygen layer

Compound	$a_t, \text{ \AA}$	$c', \text{ \AA}$	$\delta c', \%$	$\delta b_0, \%$	$c_0, \text{ \AA}$	$E_1/E_2/E_3$
$Bi_4Ti_3O_{12}$	3.899	3.64	-6.6	-1.3	4.85	1.2/0.6/0.02
$Bi_{3.8}Nd_{0.2}Ti_3O_{12}$	3.843	3.664	-4.6	-0.33	4.88	0.76/0.24/0.04

SEM analysis is shown that all compounds sintered at temperatures of 1000 and 1050 °C have a similar microstructure. There are grains of both round and oblong shape, the grain boundaries are mostly distinct. This indicates that the cleavage occurred predominantly along the grain boundaries. It can be seen that there are conglomerates of strongly bonded grains in all studied ceramics.

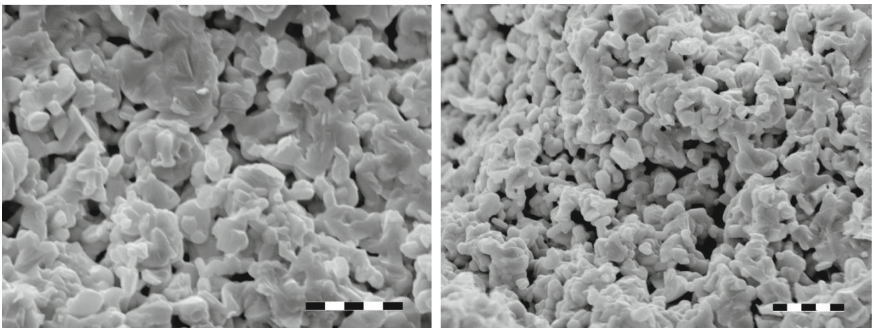


Fig. 3 Microstructure of the cleavage surface of $Bi_4Ti_3O_{12}$ ceramics after synthesis at 1000 °C at different magnifications; both scale markers are 5 μm

In the case of sintering at 1000 °C (Fig. 3), the grains have rounded edges, and their average size is $\sim 1.3 \mu\text{m}$. Grain conglomerates can be up to 6 – 7 μm in size. The size distribution has a log-normal character with a maximum frequency of occurrence (87%) of 1 – 1.8 μm (Fig. 4).

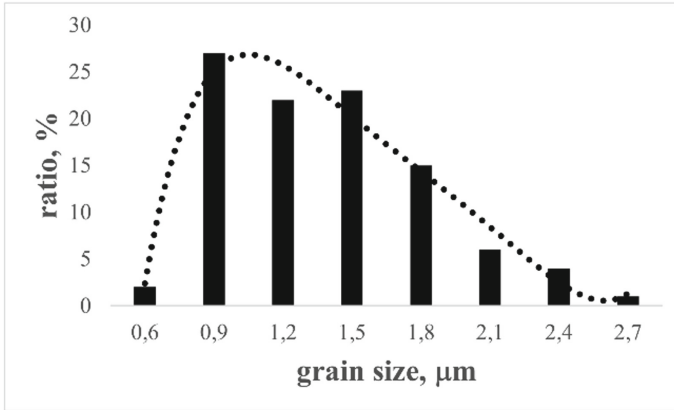


Fig. 4 Grain size distribution in $\text{Bi}_4\text{Ti}_3\text{O}_{12}$ ceramics after synthesis at 1000 °C

After synthesis at 1050 °C (Fig. 5), the grain size situation is identical. The average size remains within $\sim 1.3 \mu\text{m}$, however, their size distribution acquires a character close to Gaussian (Fig. 6). At the same time, the maximum frequency of occurrence (88%) also remains within 1 – 1.8 μm . The volume of conglomerated grains is noticeably higher, and their size in some cases reaches 8 – 9 μm .

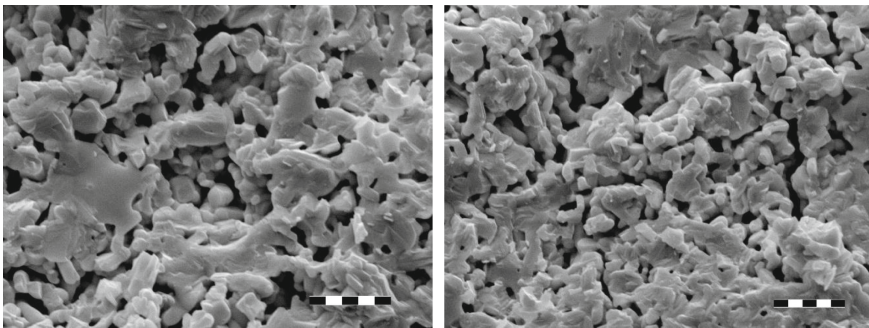


Fig. 5 Microstructure of the cleavage surface of $\text{Bi}_4\text{Ti}_3\text{O}_{12}$ ceramics after synthesis at 1050 °C at different magnifications; both scale markers are 5 μm

Figure 7 shows images of the microstructure of $\text{Bi}_{3,8}\text{Nd}_{0,2}\text{Ti}_3\text{O}_{12}$. It can be seen that the cleavage surface is quite loose, the cleavage occurred mainly along the grain boundaries. Therefore, the grain boundaries are clear. There are small areas with densely grouped crystallites, in which the cleavage went directly through the grains. In these

regions, one can see that the internal structure of the grains is homogeneous (Fig. 7, selected regions).

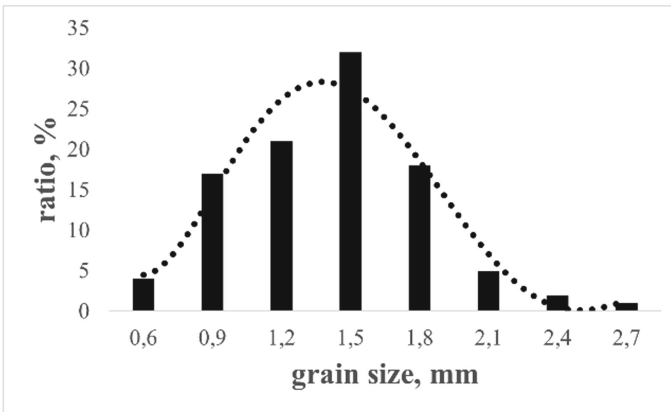


Fig. 6 Grain size distribution in Bi₄Ti₃O₁₂ ceramics after synthesis at 1050 °C

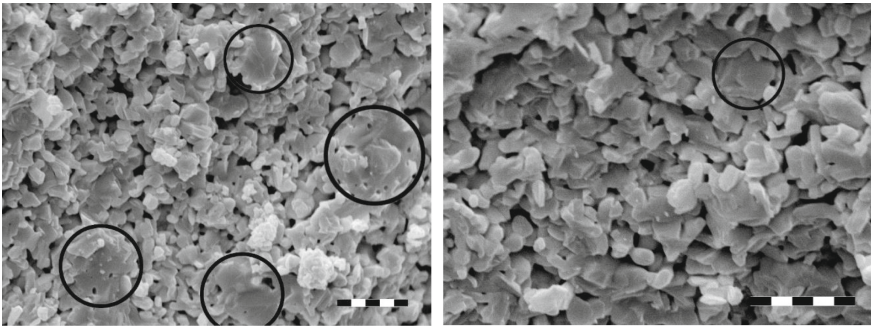


Fig. 7 Microstructure of the cleavage surface of Bi_{3,8}Nd_{0,2}Ti₃O₁₂ ceramics after synthesis at 1000 °C at different magnifications; both scale markers are 5 μm

The grains mostly have rounded edges, and their average size is ~ 1.15 μm. The size distribution has a classical log-normal character with the maximum frequency of occurrence (80%) of grains within 0.75 – 1.75 μm (Fig. 8).

After synthesis at 1050 °C (Fig. 9), the following occurs. Obviously, here the cleavage surface is denser; therefore, the cleavage occurred both along the grains and along their boundaries. The average crystallite size increases to ~ 1.45 μm. The scatter in size retains its character of log-normal distribution (Fig. 10). The regions in which cleavage occurs along the grains are characterized by the presence of lamellar grains, similar to those that form in the structure of the Aurvilius phases (Fig. 9, highlighted regions). At the same time, it can be noted that the internal structure of these lamellar crystallites is slightly inhomogeneous, which most likely indicates their layering.

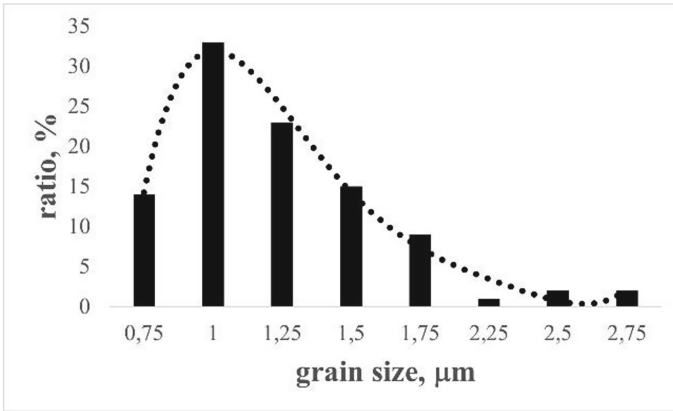


Fig. 8 Grain size distribution in $\text{Bi}_{3,8}\text{Nd}_{0,2}\text{Ti}_3\text{O}_{12}$ ceramics after synthesis at $1000\text{ }^\circ\text{C}$

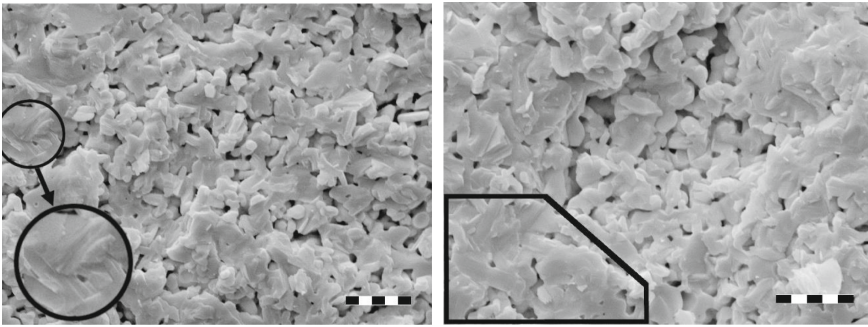


Fig. 9 Microstructure of the cleavage surface of $\text{Bi}_{3,8}\text{Nd}_{0,2}\text{Ti}_3\text{O}_{12}$ ceramics after synthesis at $1050\text{ }^\circ\text{C}$ at different magnifications; both scale markers are $5\text{ }\mu\text{m}$

Figure 11, 12 show the temperature dependences of the relative permittivity $\varepsilon/\varepsilon_0(T)$ and the dielectric loss tangent for $\text{Bi}_{4-x}\text{Nd}_x\text{Ti}_3\text{O}_{12}$ ($x = 0.0, 0.2$) at a frequency from 100 kHz to 1 MHz, sintered at temperatures of $1000\text{ }^\circ\text{C}$ and $1050\text{ }^\circ\text{C}$, respectively.

The electrical conductivity along a -axis is several orders of magnitude higher than along c -axis. Oxide ion conductivity, due to a large number of oxygen vacancies in the perovskite layers, leads to a high electrical conductivity along a -axis of about $700\text{ }^\circ\text{C}$. As it is known, with an increase in the sintering temperature, the grain sizes in the ab -direction will increase (Fig. 10), which leads to an increase in conductivity and an increase in the dielectric loss tangent (Figs. 11, b1, 12, b3).

Calculations show that the formation of Bi^{3+} vacancies occur predominantly at the A-site of the perovskite layers, rather than in the Bi_2O_2 layers, leading to oxygen vacancies in the perovskite layers [17]. The temperature dependences of the permittivity (ε') and dielectric loss tangent ($\text{tg}\sigma$) in the range from 100 kHz to 1 MHz for all compositions are shown in Figs. 11, 12. In Figs. 11, a1 – 12, a3 the T_C of the $\text{Bi}_4\text{Ti}_3\text{O}_{12}$ compositions is $\sim 711 - 715\text{ }^\circ\text{C}$, and a significant change in T_C is caused by doping with Nd^{3+} (Figs. 11,

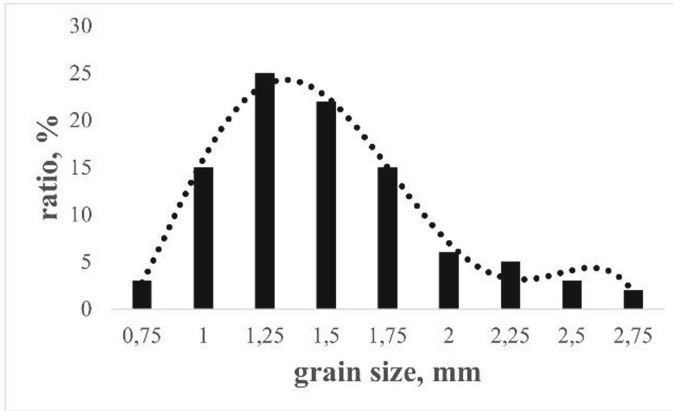


Fig. 10 Grain size distribution in ceramics $\text{Bi}_{3,8}\text{Nd}_{0,2}\text{Ti}_3\text{O}_{12}$ after synthesis at $1050\text{ }^\circ\text{C}$

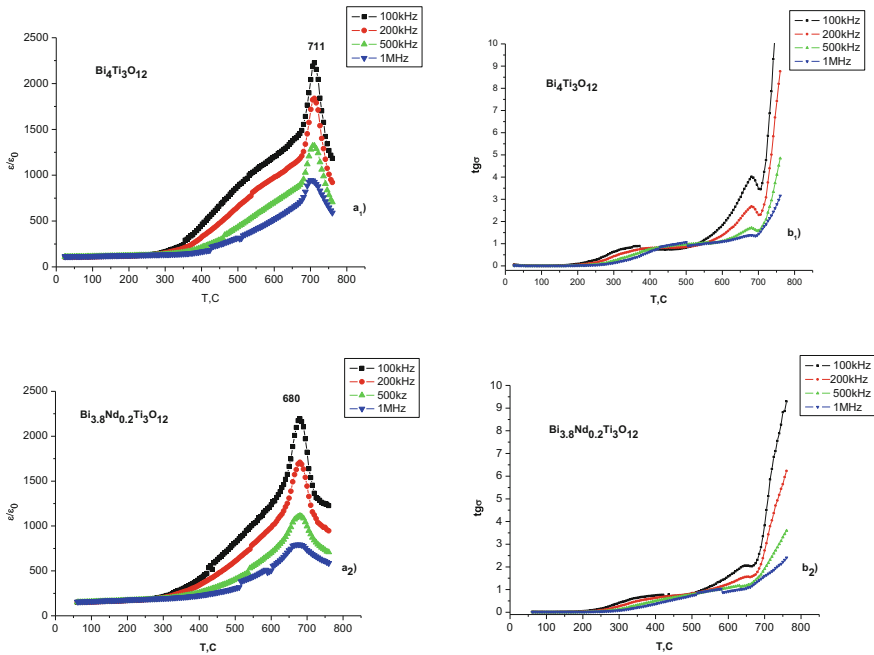


Fig. 11 Temperature dependences of relative permittivity $\varepsilon' = \varepsilon/\varepsilon_0$ (a_1 , a_2) and loss tangent $\text{tg}\sigma$ (b_1 , b_2) for APs $\text{Bi}_{4-x}\text{Nd}_x\text{Ti}_3\text{O}_{12}$ ($x = 0.0, 0.2$) at a frequency from 100 kHz to 1 MHz at a sintering temperature of $1000\text{ }^\circ\text{C}$

$a_2 - 12$, a_4) and the T_C of the $\text{Bi}_{3,8}\text{Nd}_{0,2}\text{Ti}_3\text{O}_{12}$ compositions is $\sim 680 - 685\text{ }^\circ\text{C}$. However, doping with Nd at the *B*-site does not significantly affect T_C and $\varepsilon'_{\text{max}}$ (maximum of ε'). The value of $\varepsilon'_{\text{max}}$ for $\text{Bi}_{4-x}\text{Nd}_x\text{Ti}_3\text{O}_{12}$ ($x = 0.0, 0.2$) sintered at $1050\text{ }^\circ\text{C}$ is $\sim 2800 - 4000$, which is much higher than that of $\text{Bi}_{4-x}\text{Nd}_x\text{Ti}_3\text{O}_{12}$ ($x = 0.0, 0.2$), sintered

at temperature 1000 °C (~ 2200 – 2500). Figures 11, b1 – 12, b3 $\text{Bi}_4\text{Ti}_3\text{O}_{12}$ shows an increase in the dielectric loss tangent from 1 to 6 above ~ 500 °C, and this increase is almost exponential. At the same time, $\text{Bi}_4\text{Ti}_3\text{O}_{12}$, doped with Nd (Figs. 11, b2 – 12, b4), demonstrates a decrease in the dielectric loss tangent, and its increase in the temperature range from 500 °C to 645 °C is ~ 1, and this increase has a linear dependence. Relaxation in the temperature range from 200 °C to 500 °C, associated with a wide anomaly, and, is also associated probably with the movement of oxygen anions over short distances inside the crystal [18]. Moreover, $\text{Bi}_4\text{Ti}_3\text{O}_{12}$, doped with Nd, demonstrates a shift in the beginning of the relaxation “step” toward higher temperatures from 150 to 200 °C (see Figs. 11, 12). The low-temperature dielectric anomaly depends on frequency, while for the dielectric anomaly, associated with the phase transition, no dependence on frequency is observed.

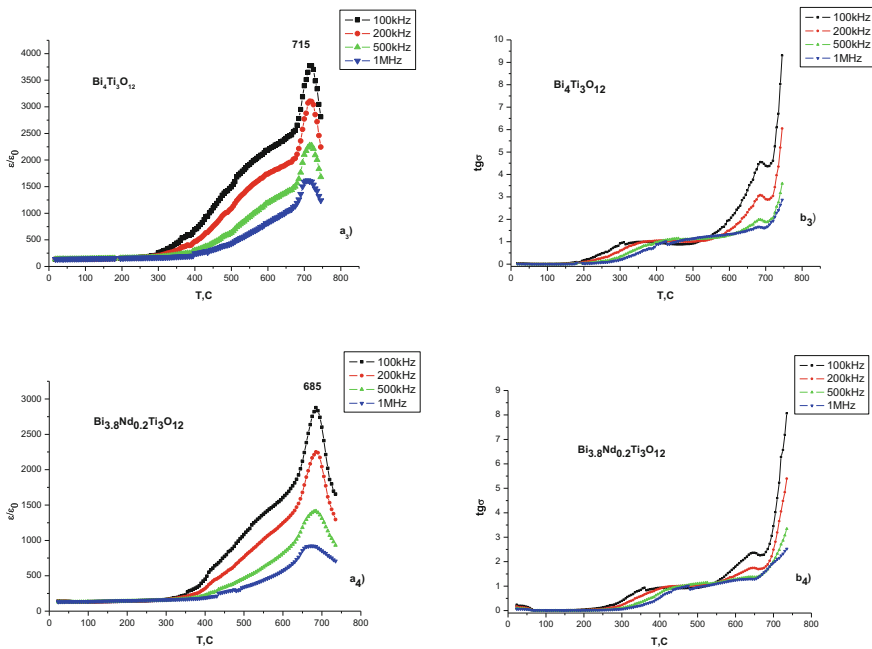


Fig. 12 Temperature dependences of relative permittivity $\varepsilon' = \varepsilon/\varepsilon_0$ (a₃, a₄) and loss tangent $\text{tg}\delta$ for APs $\text{Bi}_{4-x}\text{Nd}_x\text{Ti}_3\text{O}_{12}$ ($x = 0.0, 0.2$) at a frequency from 100 kHz to 1 MHz, at sintering temperature 1050 °C

The low temperature anomaly is probably associated with the formation of Schottky barriers between the ceramic and metal electrodes due to the difference in the Fermi level between them [19, 20].

A distinctive evolution like broadening is observed from $\text{Bi}_4\text{Ti}_3\text{O}_{12}$ to $\text{Bi}_{3.8}\text{Nd}_{0.2}\text{Ti}_3\text{O}_{12}$. This suggests that the broadening at $x = 0.2$ is not a microstructural effect, but a truly compositional effect. This is indicative of the presence of a Curie

temperature distribution, and is not necessarily due to chemical inhomogeneities, and is commonly referred to as a diffuse phase transition.

Ceramics $\text{Bi}_{4-x}\text{Nd}_x\text{Ti}_3\text{O}_{12}$ ($x = 0.0, 0.2$) have a low piezoelectric activity ($7 \text{ pC/N} \leq d_{33} \leq 8 \text{ pC/N}$) and doping with Nd did not increase the piezoelectric activity. After the polarization of the samples $\text{Bi}_{4-x}\text{Nd}_x\text{Ti}_3\text{O}_{12}$ ($x = 0.0, 0.2$), we again measured the temperature dependence of the permittivity. It was found that the Curie temperature decreased by 10°C . Thus, we can say that the presence of the sample in an electric field leads to a decrease in the Curie temperature.

The activation energy (E_a) was determined from the Arrhenius equation:

$$\sigma = (A/T)\exp[-E_a/(kT)], \quad (3)$$

where σ is the electrical conductivity, k is a Boltzmann constant, A is a constant, E_a is the activation energy. A typical dependence of $\ln\sigma$ (σ -conductivity) on $1/T$ (at a frequency of 100 kHz), which was used to determine the activation energy E_a , is shown in Fig. 4 for APs $\text{Bi}_{4-x}\text{Nd}_x\text{Ti}_3\text{O}_{12}$ ($x = 0.0, 0.2$). The $\text{Bi}_{4-x}\text{Nd}_x\text{Ti}_3\text{O}_{12}$ ($x = 0.0, 0.2$) compounds have two temperature ranges, in which the activation energy E_a differs significantly in value. In the area of low temperatures, electrical conductivity is determined mainly by impurity defects with very low activation energies of the order of several hundredths of an electron volt. For $\text{Bi}_{4-x}\text{Nd}_x\text{Ti}_3\text{O}_{12}$ ($x = 0.0, 0.2$) compounds, we observe a region with pronounced impurity conductivity in the temperature range from 20 to 200°C .

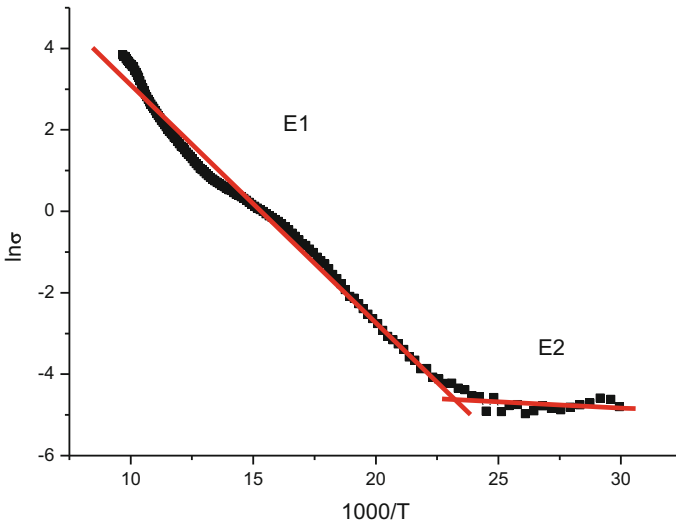


Fig. 13 Dependence of $\ln\sigma$ on $10,000/T$ for the $\text{Bi}_{4-x}\text{Nd}_x\text{Ti}_3\text{O}_{12}$ sample ($x = 0.2$) at a frequency of 100 kHz

When $\text{Bi}_4\text{Ti}_3\text{O}_{12}$ is doped with neodymium, the activation energy in the low-temperature and high-temperature regions, as follows from Table 2, practically does not change. The invariance of the activation energy indicates the constancy of the nature of conductivity in the synthesized series of compounds.

4 Conclusions

In summary, $\text{Bi}_{4-x}\text{Nd}_x\text{Ti}_3\text{O}_{12}$ ($x = 0.0, 0.2$) ceramics, were successfully prepared by a conventional solid-state reaction method. XRD patterns were identified as Aurivillius orthorhombic B2cb for all orders. As expected, Nd^{3+} doping reduced the electrical conductivity by about two orders of magnitude, compared to undoped $\text{Bi}_4\text{Ti}_3\text{O}_{12}$. The Curie temperature for $\text{Bi}_4\text{Ti}_3\text{O}_{12}$ was refined and it was $T_C = 715$ °C. The polarization of the sample resulted in a decrease in the Curie point. Doping $\text{Bi}_4\text{Ti}_3\text{O}_{12}$ with neodymium Nd^{3+} lowered the Curie temperature by 30 °C.

Acknowledgements. The equipment of SFedU and SSC RAS was used. The authors acknowledge the support by Southern Federal University, grant No. 21–19-00423 of the Russian Science Foundation.

References

1. B. Aurivillius, *Arkiv. Kemi.*, **54**, 463 (1949).
2. G. A. Smolensky, V. A. Isupov, A. I. Agranovskaya, *Soviet Physics Solid State*, 959 (1969).
3. S. V. Zubkov, S. I. Shevtsova, In: *Advanced Materials - Proceedings of the International Conference on "Physics and Mechanics of New Materials and Their Applications"*, PHENMA 2019, Springer Proceedings in Materials, Ivan A. Parinov, Shun-Hsyung Chang, Banh Tien Long (Eds.). Springer Nature, Cham, Switzerland, **6**, 173 – 182 (2020).
4. S. V. Zubkov, V. G. Vlasenko, *Physics of the Solid State*, **59**, 12, 2325 – 2330 (2017).
5. B. Park, B. Kang, S. Bu, et al., *Nature*, **401**, 682, 6754, (1999).
6. X. Chen, C. Wei, J. Xiao, et al., Room temperature multiferroic properties and magnetocapacitance effect of modified ferroelectric $\text{Bi}_4\text{Ti}_3\text{O}_{12}$ ceramic, *J. Phys. D: Appl. Phys.*, **46**, 42, 425001 (2013).
7. A. Megriche, L. Lebrun, M. Troccaz, *Sens. Actuators A: Phys.*, **78**, 2, 88 – 91 (1999).
8. Y. Chen, D. Liang, Q. Wang, et al., *J. Appl. Phys.*, **116**, 7, 074108 (2014).
9. A. Gruverman, O. Auciello, H. Tokumoto, *Ann. Rev. Mater. Sci.*, **28**, 101 - 123 (1998).
10. S. V. Zubkov, I. A. Parinov, A. V. Nazarenko, Yu. A. Kuprina, *Phys. Solid State*, **10**, 1475 (2022).
11. W. Kraus, G. Nolze, *PowderCell for Windows. Version 2.3* (Federal Institute for Materials Research and Testing, Berlin, (1999).
12. X. Du, I. Chen, *J. Am. Ceram. Soc.*, **81**, 12, 3260 (1998).
13. E. C. Subbarao, *J. Chem. Phys.*, **34**, 695 (1961).
14. V. M. Goldschmidt, *Geochemische Verteilungsgesetze der Elemente*, Norske, Oslo, (1927).
15. R. D. Shannon, *Acta Crystallogr., Sect. A*, **32**, 75 (1976).
16. V. A. Isupov, *Ferroelectrics*, **189**, 211 (1996).
17. Y. Noguchi, K. Yamamoto, Y. Kitanaka, M. Miyayama, *J. of the European Ceramic Society*, **27**, 4081 – 4084 (2007).
18. H. S. Shulman, D. Damjanovic, N. Setter, *J. Am. Ceram. Soc.* **83**, 528 – 532 (2000).
19. M. Li, Z. Shen, M. Nygren, A. Feteira, D. C. Sinclair, A. R. West, *J. Appl. Phys.* **106**, 104106 (2009).
20. C. Longa, H. Fanc, W. Ren, J. Zhao, *J. of the European Ceramic Society*, **39**, 4103 – 4112 (2019).